CCAMLR Science, Vol. 25 (2025): 1–18

Hydrologic regionalisation from Crozet to Kerguelen and subtropical Southern Indian Ocean

V. Djian[1,2,3]✉, C. Cotté[2] and P. Koubbi[2,3].

[1] Laboratoire de Biologie des Organismes et Ecosystèmes Aquatiques (BOREA)
MNHN, CNRS, IRD, SU, UCN, UA
45 rue Buffon, 75231 Paris Cedex 05
France

[2] LOCEAN-IPSL – Sorbonne Université, CNRS, IRD, MNHN, Laboratoire d'Océanographie et du Climat: Expérimentations et Approches Numériques
4, place Jussieu, Boite 100 . F-75252 Paris Cedex 05
France

[3] IFREMER Centre Manche Mer du Nord. Unité Halieutique Manche Mer du Nord
150 quai Gambetta, 62321 Boulogne-sur-Mer
France

Email: valentindjian@gmail.com

Abstract:

The islands of Crozet and Kerguelen are located at the junction of the Southern Indian Ocean and the Southern Ocean, an area of major environmental contrasts due to the juxtaposition of subtropical warm and salty waters and polar cold waters. Frontal structures generated by the Antarctic Circumpolar Current divide these oceans into several oceanographic zones. Several regionalisations have been carried out in recent decades, but only on the epipelagic or mesopelagic zones, without considering both together. As these frontal zones have a strong influence on environmental conditions and the distribution of biodiversity, it is important to be able to identify their spatial distribution and boundaries. The aim of this study was to identify the different hydrologic zones in the Indian sector of the Southern Ocean and the Southern Indian Ocean from oceanographic open access data. Temperature and salinity profiles from the surface to 1000 m depth between 2010 and 2020 were retrieved from Copernicus reanalyses. A functional PCA was applied to these data to account for the defined depth of the water column, followed by k-means clustering to identify regions with common hydrologic profile. We also calculated the mean and standard deviation of the cluster value for each geographical cell to identify stable areas and areas of high hydrologic variability. Each region was then linked to environmental data from the whole study area to characterise it. We were able to identify 7 regions, 4 in the Southern Indian Ocean and 3 in the Southern Ocean. The regions in the Southern Ocean are strongly explained by the frontal zones such as the Subantarctic and Polar fronts. Conversely, the regions in the Southern Indian Ocean are explained by differences in salinity, particularly in subsurface waters, associated with the action of the South Equatorial Current.

Résumé

Les îles Crozet et Kerguelen sont situées à la croisée du sud de l'océan Indien et de l'océan Austral, une zone marquée par de forts contrastes environnementaux en raison de la juxtaposition d'eaux subtropicales chaudes et salées et d'eaux polaires froides. Les structures frontales générées par le courant circumpolaire antarctique divisent ces océans en plusieurs zones océanographiques. Plusieurs régionalisations ont été effectuées au cours des dernières décennies, mais uniquement dans les zones épipélagiques ou mésopélagiques, sans tenir compte des deux zones considérées de manière conjointe. Ces zones frontales ayant une forte influence sur les conditions environnementales et la répartition de la biodiversité, il est important de pouvoir identifier leur distribution spatiale et leurs limites. L'objectif de cette étude est d'identifier les différentes zones hydrologiques dans le secteur indien de l'océan Austral et dans le sud de l'océan Indien à partir de données océanographiques en libre accès. Les profils de température et de salinité de la surface à 1000 m de profondeur entre 2010 et 2020 ont été extraits des réanalyses des services Copernicus. Une analyse en composantes principales (ACP) fonctionnelle a été appliquée à ces données afin de tenir compte de la profondeur définie de la colonne d'eau, suivie d'un regroupement par la méthode des k-moyennes afin d'identifier les régions présentant un profil hydrologique commun. Nous avons également calculé la moyenne et l'écart-type de la valeur de l'agrégat pour chaque cellule géographique afin d'identifier les zones stables et les zones à forte variabilité hydrologique. Chaque région a ensuite été reliée aux données environnementales de l'ensemble de la zone d'étude afin de la caractériser. Nous avons pu identifier sept régions, quatre dans le sud de l'océan Indien et trois dans l'océan Austral. Les régions de l'océan Austral sont fortement influencées par les zones frontales telles que les fronts subantarctiques et polaires. À l'inverse, les régions du sud de l'océan Indien s'expliquent par des différences de salinité, notamment dans les eaux sous-marines, associées à l'action du courant équatorial sud.

Абстракт

Острова Крозе и Кергелен расположены на стыке южной части Индийского океана и Южного океана, в районе, характеризующемся значительными экологическими контрастами из-за соседства субтропических теплых и соленых вод и полярных холодных вод. Фронтальные структуры, образующиеся под воздействием Антарктического циркумполярного течения, разделяют эти океаны на несколько океанографических зон. В последние десятилетия было проведено несколько регионализаций, однако только в отношении эпипелагической или мезопелагической зон, без учета обоих типов зон в совокупности. Поскольку эти фронтальные структуры оказывают значительное влияние на условия окружающей среды и распределение биоразнообразия, важно иметь возможность определять их пространственное распределение и границы. Целью данного исследования было выявление различных гидрологических зон в индийском секторе Южного океана и южной части Индийского океана на основе океанографических данных, находящихся в открытом доступе. Статистика показателей температуры и солености от поверхности до глубины 1 000 м в период с 2010 по 2020 год была получена из повторных анализов Copernicus. К этим данным был применен функциональный анализ главных составляющих с учетом заданной глубины водной толщи, а затем была проведена кластеризация методом k-средних для определения регионов с общим гидрологическим профилем. Мы также рассчитали среднее значение и стандартное отклонение кластерного значения для каждой географической ячейки, чтобы выявить стабильные районы и районы с высокой гидрологической изменчивостью. Затем каждый регион был сопоставлен с экологическими данными по всему району исследования для его характеристики. Нам удалось выделить семь (7) регионов: четыре (4) в южной части Индийского океана и три (3) в Южном океане. Регионы Южного океана в значительной степени определяются фронтальными структурами, такими как субантарктические и полярные фронты. Напротив, особенности регионов южной части Индийского океана обусловлены различиями в солености, особенно в приповерхностных водах, связанными с действием Южного экваториального течения.

Resumen

Las islas Crozet y Kerguelén están situadas en la confluencia del océano Índico Meridional y del océano Austral, una zona de grandes contrastes medioambientales debido a la yuxtaposición de aguas cálidas y saladas subtropicales y aguas frías polares. Las estructuras frontales generadas por la Corriente Circumpolar Antártica dividen estos océanos en varias zonas oceanográficas. En las últimas décadas se han llevado a cabo varias regionalizaciones, pero sólo de las zonas epipelágicas o mesopelágicas, sin considerar ambas conjuntamente. Dado que estas zonas frontales tienen una gran influencia en las condiciones medioambientales y en la distribución de la biodiversidad, es importante poder identificar su distribución espacial y sus límites. El objetivo de este estudio era identificar las diferentes zonas hidrológicas del sector indio del Océano Austral y del Océano Índico Meridional a partir de datos oceanográficos de libre acceso. Se obtuvieron los perfiles de temperatura y salinidad en la capa desde la superficie hasta los 1000 m de profundidad entre 2010 y 2020 de los reanálisis de Copernicus. Se aplicó a estos datos un análisis de componentes principales (PCA) funcional para dar cuenta de la profundidad definida de la columna de agua, seguido de un agrupamiento de k-medias para identificar regiones con perfiles hidrológicos comunes. También calculamos la media y la desviación estándar del valor de agrupación de cada celda geográfica para identificar las zonas estables y las zonas de gran variabilidad hidrológica. A continuación, se caracterizó cada región relacionándola con los datos medioambientales de toda la zona de estudio. Se consiguió identificar 7 regiones, 4 en el Océano Índico Meridional y 3 en el Océano Austral. Las regiones del Océano Austral se explican en gran medida por las zonas frontales, como los frentes subantártico y polar. Por el contrario, las regiones del Océano Índico Meridional se explican por las diferencias de salinidad, sobre todo en las aguas subsuperficiales, asociadas a la acción de la Corriente Ecuatorial del Sur.

Introduction

The North Indian sector of the Southern Ocean and the Southern Indian Ocean are areas with contrasting physico-chemical characteristics within a small latitudinal range of a dozen degrees. The Southern Indian Ocean is oligotrophic and characterised by warm and saline waters. To the west of it, at its limit with the Southern Ocean, it is influenced by the Agulhas Return Current (ARC, Fig. 1, Lutjeharms and Ansorge, 2001; Lutjeharms and da Silva, 2019). South of it, the Southern Ocean has much colder waters and higher nutrient concentrations. In its northern part, primary production is strongly limited by bioavailable iron, except in the vicinity of islands and seamounts (Doty and Oguri, 1956; Blain et al., 2007). This ocean can be divided into several hydrologic zones (Park et al., 1991; Orsi et al., 1995; Post et al., 2014) defined by the presence of hydrologic fronts related to the Antarctic Circumpolar Current (ACC), a current of very high intensity close to 100 Sv eastward (Orsi et al., 1995). The fronts may be constrained by topography, such as oceanic ridges or island shelves. The Subtropical Front (STF) corresponds to the zone where the subtropical surface waters (STSW) coexist with the less warm and saline subantarctic surface waters (SASW). The proximity of these two water masses creates a significant environmental gradient, with a temperature difference of 4–5°C and a salinity of 0.5 psu at the level of this front (Deacon, 1982). The STF marks the boundary between the Subtropical Zone (STZ) to the north of it and the Subantarctic Zone (SAZ) to the south of it. The SAZ is influenced in its latitudinal extent by the subantarctic island shelves. This is the case north of the Kerguelen Plateau, where the juxtaposition of the STF and the SAF, caused by the influence of topography, limits the SAZ to a 2° latitude band called the Transitional Frontal Zone (Gambéroni et al., 1982; Charriaud and Gamberoni, 1987; Park et al., 1991 and 1993). This is also the case north of the Crozet Plateau, where the confluence of the ARC, STF and Subantarctic Front (SAF) forms the Crozet Triple Front (Belkin and Gordon, 1996). The SAF separates the SAZ from the Polar Frontal Zone (PFZ). The latitudinal extent of the PFZ is limited near Kerguelen because the PFZ rises northeast of the island shelf. Zones of high chlorophyll concentration are observed around Crozet and Kerguelen Islands, whose shelves, coupled with continental run-off, favour primary production by enriching the environment with nutrients and iron, a limiting element for primary production in the Southern Ocean (Doty and Oguri, 1956; Blain et al., 2007). Finally, further south, the Antarctic Zone (AZ) is the zone with the northern boundary of the PF, a high nutrient low chlorophyll (HNLC) zone where productivity is limited by low iron concentration despite high concentration of nitrates and phosphates. This region lies north of the sea-ice zone that borders the Antarctic continent and is also called the Permanent Open Ocean Zone.

This zonation based on hydrologic structures is not the only one that has been carried out in the Southern Ocean and Southern Indian Ocean. Several bioregionalisation studies have been carried out on surface waters, considering environmental parameters and chlorophyll concentration (Longhurst, 2010; Godet et al., 2020). The epipelagic regionalisation carried out by Longhurst (2010) gives relatively similar results to the zonation based on hydrologic structures, with the definition of 4 epipelagic provinces along a latitudinal gradient. The first two correspond to a subdivision of the subtropical regime between the 'Indian South Subtropical Gyre' (ISSG) province, with an oligotrophic regime linked to the Indian subtropical gyre, and the 'South Subtropical Convergence' (SSTC) province, characterised by strong turbulence and high chlorophyll-a enrichment. The last two correspond to a separation between a chlorophyll-rich regime within the 'Subantarctic Water Ring' (SANT) province, integrating both the SAZ and PFZ, and a HNLC regime within the 'Antarctic' (ANTA) province south of the PF. Another regionalisation based on the analysis of mesopelagic biogeochemical parameters was performed by Reygondeau et al. (2018), which also observed a latitudinal gradient. In our area of interest, the subtropical zone is subdivided into different biogeochemical provinces, one related to the Indian subtropical gyre called the 'Subtropical Gyre Province', one related to the subtropical front called the 'Southern Subtropical Frontal Province', and a last one called the 'Subtropical Province'. The Southern Ocean is subdivided into a 'Southern Ocean Temperate Province', a 'Sub-Polar Province' and a 'Cold and Oxic Polar Province'. However, these different regionalisations are defined either to the epipelagic or the mesopelagic layer and do not include the whole water column which will be the aim of this paper.

Functional Principal Component analysis (fPCA, Ramsay and Silverman, 2015) is an approach that can be used to characterise the water column as a whole, particularly for regionalisation purposes. It consists of analysing the simultaneous variations of temperature and salinity profiles as a function of depth, described as continuous functional curves using a decomposition in a B-spline basis for each spatial position (Pauthenet et al., 2017) which are then analysed using the fPCA. Its interest is to be able to decouple the phenomena that governs the types of the vertical profiles and to quantify the variance that they induce on the structure of the water column, while considering the latter as a whole. This approach has been used to study 3D hydrographic structures (Pauthenet et al., 2017; Kolbe et al., 2021) and 3D acoustic structures (Ariza et al., 2022, 2023). It is therefore possible to carry out a regionalisation based on the 3D structure of the water column by using a clustering approach on the fPCA results and thus compare it to previous regionalisations in the Southern Ocean and the Southern Indian Ocean.

In this study, we therefore sought to determine the 3D hydrologic structure of the area between Crozet, Kerguelen and St Paul and New Amsterdam islands. To do this, we performed a regionalisation based on the results of a functional principal component analysis on temperature and salinity profiles in order to identify hydrologic regions of common hydrology.

Material and methods

Environmental data

Oceanographic data to explain species distribution from the REPCCOAI summer surveys (Response of the pelagic ecosystem to climate change in the Southern Ocean and Southern Indian Ocean) were retrieved from 2010 to 2020 from the beginning of January to the end of February (Figure 1). Monthly values of several environmental parameters (from the surface to 1000 m depth) were extracted from different databases (Supplementary Table 1). Among these parameters, we extracted the temperature, salinity and oxygen concentration as indicators of water masses and chlorophyll as indicators of productive areas. We also computed kinetic energy to characterise dynamic areas like those with strong currents, such as the ACC or the Agulhas Return Current (ARC). Kinetic energy was computed from zonal and meridional velocity using the formula:

$$KE = \frac{0.5x(u^2 + v^2)}{1000} \quad (1)$$

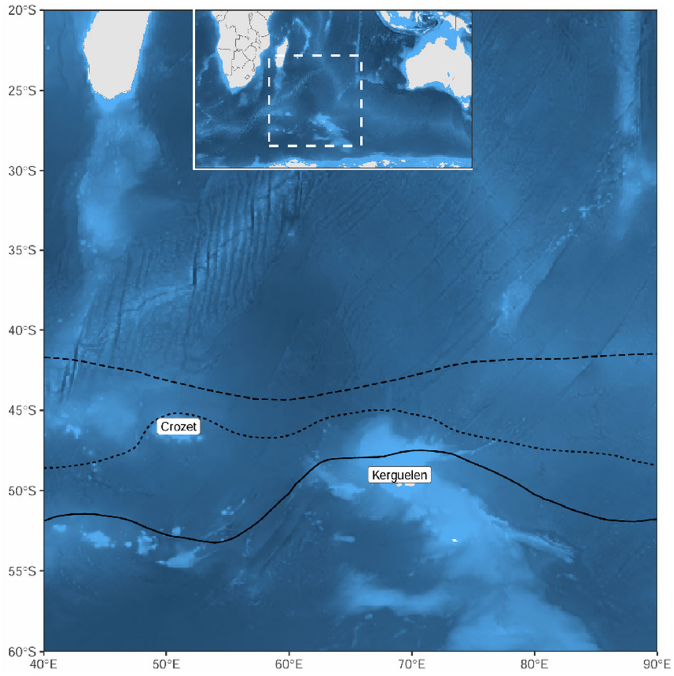

Figure 1: Map of the Indian sector of the subantarctic where the REPCCOAI surveys took place. The lines represent the fronts resulting from the ACC. The subtropical front is shown as a dashed line, the Subantarctic Front as a dotted line and the Antarctic Polar Front as a solid line.

Region identification via functional analysis

To identify hydrologic regions within our study area, a fPCA (Ramsay and Silverman, 2015) of temperature and salinity vertical profiles from the surface to 1000 m depth and from 2010 to 2020 was undertaken using the R package fda.oce (0.1.0, Pauthenet and Nerini, 2023). The fPCA differs from Principal Component Analysis in that it groups observations according to the shape of the hydrologic profiles and not only to the value of one parameter at one depth. This is achieved by interpolating the profiles according to a uniform depth scale between profiles (Pauthenet et al., 2017). A k-means classification was applied on the scores of the four first vertical thermohaline modes of the fPCA to determine clusters of vertical temperature and salinity profiles. The number of k-means clusters was determined via the gap statistic (Tibshirani et al., 2001). We computed the mean and standard deviation of cluster value for each cell from 2010 to 2020 and then mapped both to visualise the hydrologic regions identified by the method and their variability across the 2010–2020 time period. High standard deviation values mean changes in assigned hydrologic regions over geographic cells, whereas low to null standard deviation shows stability in assigned hydrologic regions. As such, high standard deviation areas should reflect transition zones between hydrologic regions, such as oceanographic fronts. We identified profile structures associated to each side of the thermohaline modes by reconstructing salinity and temperature profiles for positive and negative values on these thermohaline modes.

To characterise the hydrologic regions obtained, mean temperature-salinity diagrams (T-S diagrams) were made for each hydrologic region identified to identify potential water masses according to Anilkumar et al. (2006). To further describe them in terms of environmental characteristics, we joined hydrologic regions identified over the 2010–2020 year period with sea temperature and salinity, oxygen concentration, kinetic energy, mix-layer depth and chlorophyll-a values over the same year period according to geographic position and by year. Violin-plots of each environmental variable for each hydrologic region over the 2010–2020 period were then made and Kruskal-Wallis tests with post-hoc Mann-Whitney tests were performed to determine if environmental differences between hydrologic regions were significant for each variable.

Table 1: Characteristics of water masses according to Anilkumar et al. (2006).

Water body	Temperature (°C)	Salinity (psu)
Subtropical Surface Waters (STSW)	> 12	> 35.1
Subantarctic Surface Waters (SASW)	9	< 34
Antarctic Surface Waters (AASW)	< 5	< 34
Antarctic Intermediate Waters (AAIW)	~ 4,4	~34.42
Mode Waters (MW)	11 - 14	35 - 35.4

Results

Hydrologic regions identification

The functional PCA distinguishes temperature and salinity profiles on the four first thermohaline modes. The first thermohaline mode explains 92.67% of the total variance of the dataset and the second 3.93%. The first plane explains 96.6% of the total variance (Fig. 1a), whereas the plane of the second and third thermohaline modes explains 5.58% (Fig. 1b) and the plane of the third and fourth thermohaline modes only 2.57% (Fig. 1c).

The K-means clustering analysis made on the results of the functional PCA identified 7 hydrologic regions (Figure 2) numbered following the latitudinal gradient (Figure 4a). The first thermohaline mode is representative of the latitudinal gradient (Figure 2a) and opposes vertical profiles with high surface temperature and salinity (Figure 3a in blue) against low temperature and salinity (Figure 3a in red). The second thermohaline mode is mainly driven by salinity, accounting for 69% of the variance (Figure 3b). It opposes salinity vertical profiles that show a rapid increase shallower than 150 m depth, followed by a plateau and a slow decrease with depth (Figure 3b in blue) and salinity vertical profiles that increase to a maximum at about 200 m depth and then slowly decrease with depth (Figure 3b in red). We find hydrologic regions 4, 5 and 6 (Figure 2b in light yellow, light green and light blue respectively) at the left of the second thermohaline mode and hydrologic regions 3 and 7 (Figure 2b in light orange and blue) on the right of this thermohaline mode. The third thermohaline mode opposes hydrologic region 1 (Figure 2c in red) to the other regions. It is also mainly driven by salinity, accounting for 63% of the variance (Figure 3c). It contrasts salinity profiles with lower surface salinity, which show a sharp increase in salinity until about 250 m depth and then a decrease (Figure 3c in blue), with salinity profiles that show a slight but continuous decrease in salinity with depth (Figure 3c in red). Finally, the fourth thermohaline mode opposes hydrologic region 2 (Figure 2c in orange) to hydrologic regions 3 and 4 (Figure 2c in orange and yellow). It seems to be equally driven by temperature (44% of the variance) and salinity (56% of the variance), although the temperature profiles don't seem to be distinguishable (Figure 3d). The salinity profiles are contrasted between a strong salinity increase to about 200 m depth followed by a continuous decrease (Figure 3d in red) and a slow salinity increase to about 300 m depth followed by a continuous decrease (Figure 3d in blue).

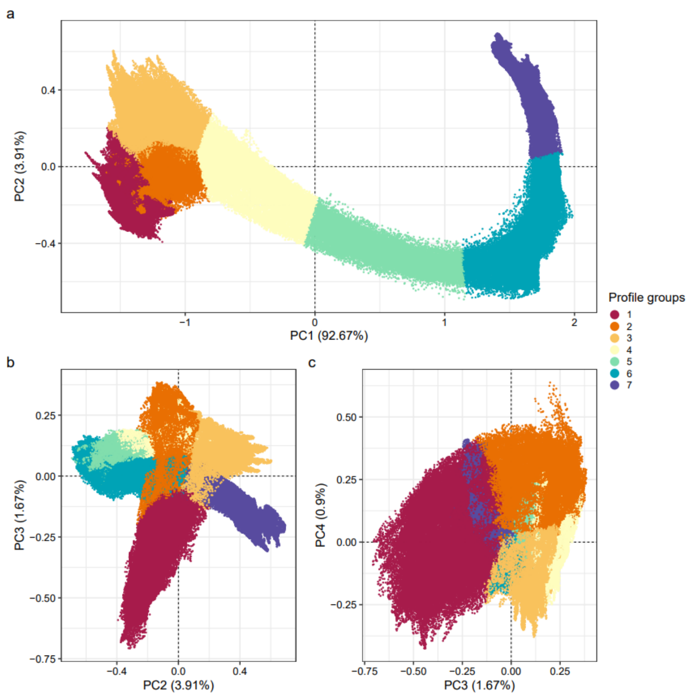

Figure 2: Scatterplot of fPCA on all temperature and salinity profiles for the planes made of a) the first and second thermohaline modes, b) second and third thermohaline modes and c) third and fourth thermohaline modes. K-means clusters are also shown on each plane.

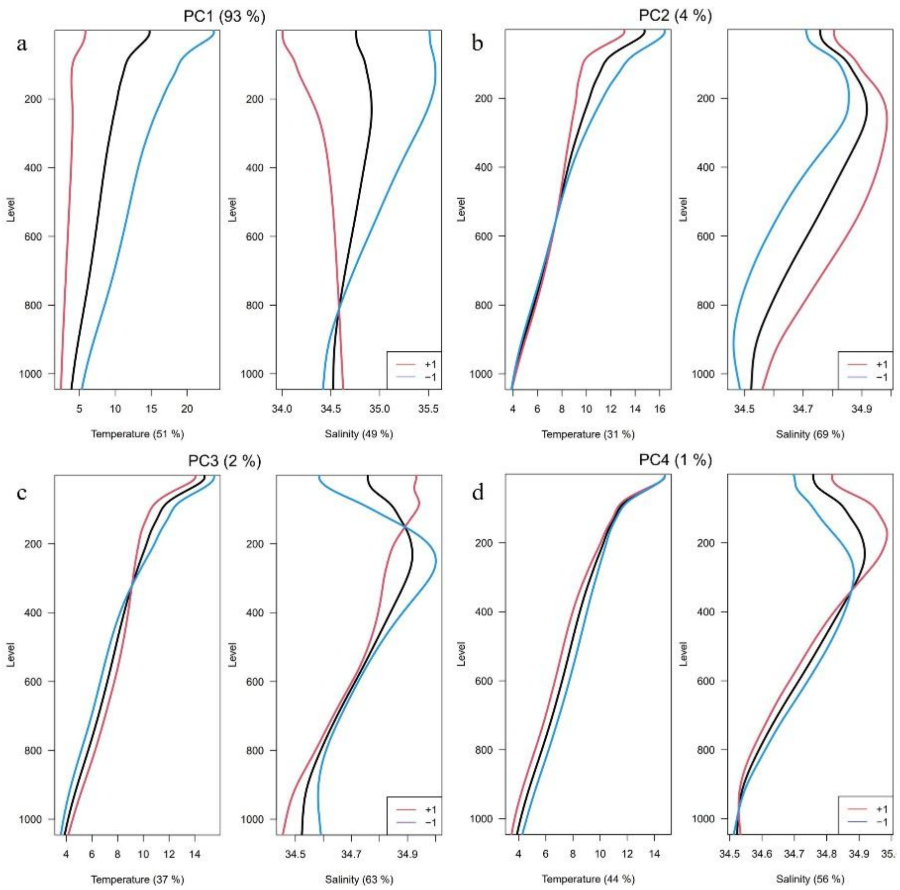

Figure 3: Reconstruction of temperature and salinity profiles for a) the first, b) the second, c) the third and d) the fourth thermohaline mode. The black profile represents the mean profile, blue, the profile for a negative value, and red for a positive value on the thermohaline mode.

The mapping of the mean cluster value from the 10 years for each geographic cell (Figure 4a) shows that the profiles of the Southern Indian Ocean are divided into four hydrologic regions. The first is hydrologic region 1, (Figure 4a in red) with its southern border reaching 30°S in the western part and rising up to 25°S in the eastern part. Hydrologic region 2 (Figure 4a in orange) is only observed in the eastern part of our study area. Its northern border is observed around 25°S and its southern border is close to 35°S from 90°E to 70°E, where it extends to 28°S. On the opposite, hydrologic region 3 (Figure 4a in light orange) is a 10° broad band only observed in the western part of our study area. Its northern border is at 30°S from 40°E to 55°E, where it extends to 35°S towards 70°E. The last of the Southern Indian Ocean hydrologic regions is hydrologic region 4 (Figure 4a in light-yellow). It corresponds to a very thin band of one degree wide in the west, which widens abruptly from 60°E to a width of about ten degrees in the east. For the Southern Ocean's profiles, we can identify three distinct hydrologic regions. The first one is hydrologic region 5, a narrow band above Crozet and Kerguelen islands South of 42°S (Figure 4a in light green). The second Southern Ocean region is hydrologic region 6, a wide band of about 8 degrees in the west, narrowing after Kerguelen Island to a band of about 2 to 5 degrees (Figure 4a in green). Its southern border has a southward boundary of 55°S and extending from 55°S to 50°S at the level of the Kerguelen Plateau. East of that, it extends southward again to 55°S. The last of the Southern Ocean hydrologic regions is hydrologic region 7, a broad band below 50°S (Figure 4a in blue), extending to the north at Kerguelen Island.

The mapping of the standard deviation of the cluster value allows us to identify transition structures between the different hydrologic regions we described above (Figure 4b). We can observe higher values of standard deviation limited to a very thin latitudinal band at the boundary between hydrological region 4 (Figure 4a in light yellow) and hydrological region 5 (Figure 4a in light green) at 40°S. The same thin band of high standard deviation is observed at the boundary between hydrological region 5 (Figure 4a in light green) and hydrological region 6 (Figure 4a in blue), starting just above 45°S in the west and moving slightly southwards towards 48°S east of the Kerguelen Islands. It is also observed at the boundary between hydrological region 6 (Figure 4a in light blue) and hydrological region 7 (Figure 4a in blue), starting at 50°S west of the Indian sector, moving down to 55°S to then sharply move northward around the Kerguelen Island shelf to finally return to 55°S. The highest values of standard deviation are observed at the boundary between hydrological region 1 (Figure 4a in red) and hydrological region 3 (Figure 4a in light orange), at the boundary between hydrological region 2 (Figure 4a in orange) and hydrological region 4 (Figure 4a in light yellow) and at the boundary between hydrological region 3 and hydrological region 4. In contrast to the boundaries between hydrological regions 5, 6 and 7 discussed above, the standard deviation values are observed over wider latitudinal bands (4–5°).

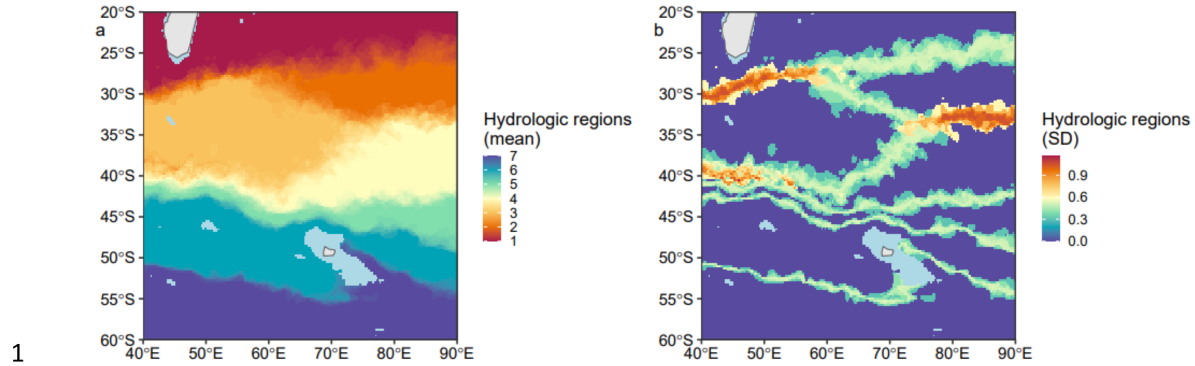

Figure 4: Mapping of a) mean and b) standard deviation of hydrologic cluster value for each cell between 2010 and 2020 identified by fPCA.

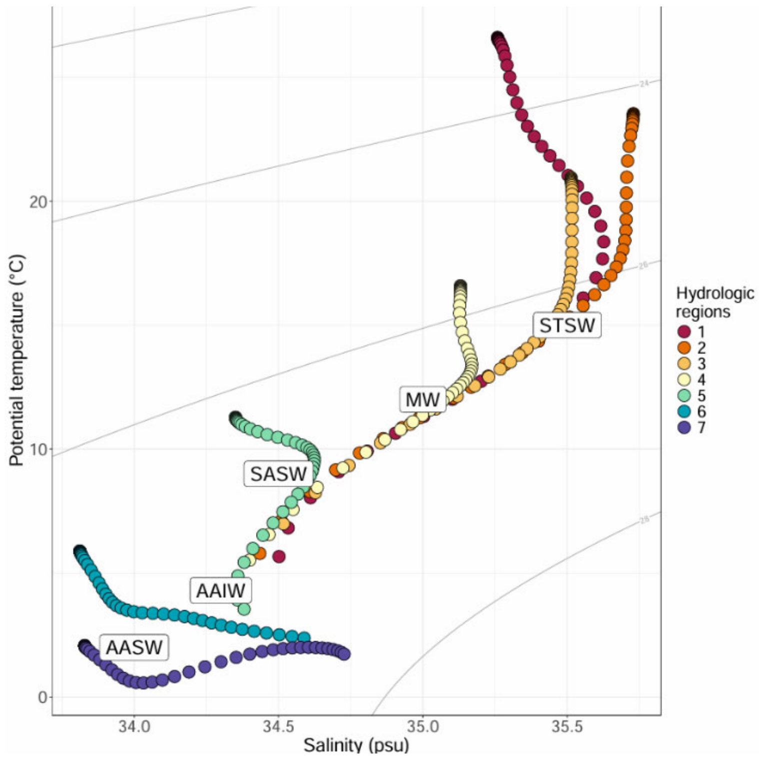

Figure 5: Temperature-Salinity diagram of mean temperature and salinity profiles from the surface to 1000 m depth for each hydrologic cluster identified (from 1 to 7) by k-means clustering on the scores of the first four thermohaline modes of the fPCA. The water bodies represented are: Subtropical Surface Waters (STSW), Subantarctic Surface Waters (SASW), Antarctic Surface Waters (AASW), Antarctic Intermediate Waters (AAIW) and Mode Waters (MW).

The T-S diagram of mean temperature and salinity profiles for each hydrologic region allows us to characterise their thermohaline structure. The mean thermohaline profile of hydrologic region 1 (Figure 5 in red) shows a water mass 10°C warmer than subtropical surface waters (STSW, Table 1), its temperature reaching 26°C. This water mass is of similar salinity, or even lower, than the STSW. Deeper waters tend to match thermohaline characteristics of mode waters (MW, Table 1). Hydrologic region 2 (Figure 5 in orange) has surface waters slightly warmer and saltier than STSW, with salinities above 35.8 psu, and deeper waters similar to MW. Hydrologic region 3 (Figure 5 in light orange) has surface waters warmer than STSW, but similar in salinity. Its deeper waters are also similar to the ones of the previous regions. Hydrologic region 4 (Figure 5 in light-yellow) shows surface waters of lower salinity than STSW, but of similar temperature. Its deeper waters are similar to MW, just as the previous regions. Hydrologic region 5 (Figure 5 in light green) distinguishes itself from the previous ones by its surface waters closer to subantarctic surface waters (SASW, Table 1) than to STSW, with temperature close to 10°C and salinity close to 34.5 psu. Its deeper waters also distinguish themselves from the previous regions by being closer to the Antarctic intermediate waters (AAIW, Table 1), with temperature being slightly lower than 5°C and salinity slightly lower than 34.5 psu. Surface waters hydrologic region 6 (Figure 5 in light blue) appear close to Antarctic surface waters (AASW, Tab. I), with temperature slightly higher than 5°C and salinity slightly higher than 33.5 psu. Its deeper waters are also similar to AAIW, except for a slightly lower temperature around 4°C. Hydrologic region 7 (Figure 5 in blue) is very similar to the previous one in terms of salinity and only differs in surface temperature being closer to 1°C than AASW and the sixth region's surface waters.

Environmental description of hydrologic regions

The Kruskal-Wallis test and Mann-Whitney post-hoc tests all showed a significant difference in sea surface temperature between the different hydrological regions (p-values < 0.001). There is a clear latitudinal gradient in sea surface temperature from hydrological region 1 (Figure 6a in red) to hydrological region 7 (Figure 6a in blue). Surface oxygen concentration shows an inverted latitudinal gradient, with Kruskal-Wallis and Mann-Whitney post-hoc tests showing a significant difference between hydrological regions (p-values < 0.001). Surface salinity tests show a significant difference between all hydrological regions (p-values < 0.001). Surface salinity is higher in hydrological region 2 (Figure 6b in orange) than in hydrological region 1 (Figure 6b in red) and then decreases until hydrological region 7 where it reaches 33 psu (Figure 6b in blue). Regarding kinetic energy, we observed a significant difference between all hydrological regions (p-values < 0.001) except between hydrological region 2 (Figure 6d in orange) and hydrological region 7 (Figure 6d in blue). Hydrological region 1 (Figure 6d in red) and hydrological region 5 (Figure 6d in light green) are the regions with the highest mean kinetic energy, while hydrological regions 2 (Figure 6d in orange) and 7 (Figure 6d in blue) have the lowest kinetic energy values. We can see an increase in kinetic energy along the latitudinal gradient from hydrological region 2 to hydrological region 5, followed by a decrease to hydrological region 7. The same trend is observed for the maximum values observed per hydrological region, with hydrological regions 2 and 5 exceeding 4.10^{-4} m^2s^{-2}. Mixed layer depth varies in a similar way to kinetic energy, with hydrological region 1 (Figure 6e in red) having a higher mean mixed layer depth than hydrological region 2 (Figure 6e in orange). This is followed by an increase in mean mixed layer depth along the latitudinal gradient (p-values < 0.001 for Kruskal-Wallis test and all post-hoc comparisons), with the latter being highest in hydrological region 7 at around 90 m (Figure 6e in blue). However, the highest maximum values of mixed layer depth are observed in hydrological region 5 (Figure 6e in light green), where it exceeds 125 m. The mean surface chlorophyll-a concentration increases along the latitudinal gradient (p-values < 0.001 for Kruskal-Wallis test and all post-hoc comparisons) from hydrological region 1 (Figure 6f in red) to hydrological region 5 (Figure 6f in light green). The mean surface chlorophyll a concentration of hydrological region 6 (Figure 6f in light blue) is slightly lower than that of hydrological region 5, while the mean surface chlorophyll a concentration of hydrological region 7 (Figure 6f in blue) is the highest. Nevertheless, the highest maximum chlorophyll concentration values are observed in hydrological region 5, with values exceeding 1.25 mg m^{-3}.

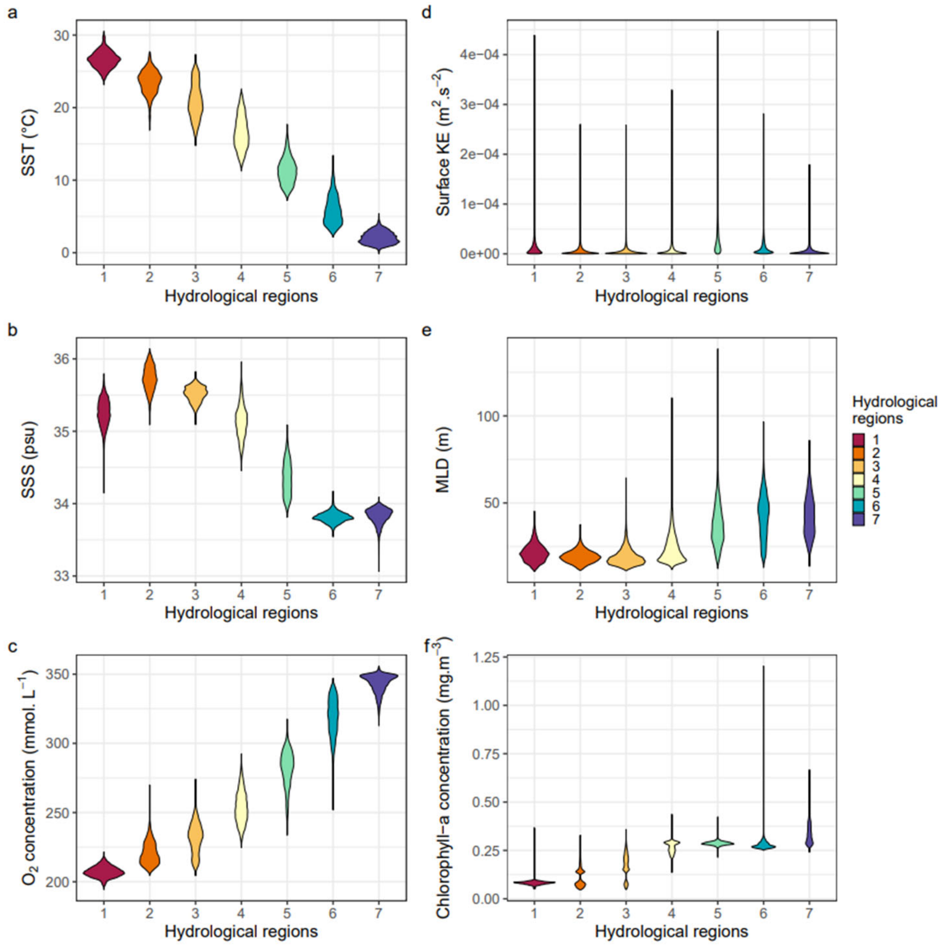

Figure 6: Violin-plots of a) sea surface temperature (SST), b) sea surface salinity (SSS), c) surface oxygen concentration, d) sea surface kinetic energy (KE), e) mixed layer depth (MLD) and f) surface chlorophyll-a concentration for each cluster identified by k-means analysis on the scores of the first four thermohaline modes of the fPCA.

Discussion

The fPCA allowed us to describe the latitudinal zonation of hydrologic properties from the tropical to the Antarctic zones. The latitudinal zonation obtained with this method completes those obtained by previous studies in the Southern Ocean (Longhurst, 2010; Reygondeau et al., 2018) which were done either on the epipelagic or the mesopelagic zones. However, unlike these studies, the use of functional analyses on temperature and salinity vertical profiles allow to capture environmental variability across the entire water column by comparing the shape of the vertical hydrologic profiles and identifying whether salinity or temperature drives the thermohaline modes obtained by the analysis (Pauthenet et al., 2017). Furthermore, the calculation of the mean and the interannual standard deviation of the cluster value from 2010 to 2020 for each geographical cell allows us to distinguish stable hydrologic regions from transition zones.

Southern Ocean hydrologic regions

The Southern Ocean hydrologic regions defined by the k-means clustering on the fPCA's principal components scores clearly match the zonation defined by the major oceanic fronts resulting from the ACC and described by Orsi et al. (1995). Hydrologic region 5 (Figure 4a in light green) matches the spatial distribution of the Subantarctic Zone (SAZ), being restricted to a narrow band because of the effect of topography on oceanic circulation, joining together the STF and the SAF. The high standard deviation observed at its northwestern border (Figure 4b) seems to match the spatial position of the 'Triple Crozet Front' at the north of Crozet Island (Charriaud and Gamberoni, 1987; Belkin and Gordon, 1996), caused by the junction of the SAF, the STF and the ARC. Moreover, the proximity between the northern and southern boundaries of the fifth hydrologic region to the north of the Kerguelen Islands is consistent with the description of the frontal transition zone, formed by the proximity between the STF and SAF (Park et al., 1991, 1993), allowing us to identify the STF and SAF as the high standard deviation bands corresponding to SAZ's borders. The oceanic circulation strongly influences this hydrologic region and is reinforced by the high values of kinetic energy and mixed layer depth observed (Figure 6d and e in light green). Values of other environmental variables are also coherent with previous descriptions of the SAZ from Racapé et al. (2010) and Orsi et al. (1995), with summer surface temperature ranging from 15 to 8°C, sea surface salinity ranging between 35 and 33.8 psu. The SAZ is grouped by Racapé et al. (2010) with the Polar Frontal Zone (PFZ) by their high chlorophyll-a concentrations. This definition matches with hydrologic region 6 (Figure 4a in light blue), the latter having the highest chlorophyll-a concentrations observed in all hydrologic regions, with maximum concentrations almost reaching 1.25 mg m^{-3} (Figure 6f in light blue). These higher concentrations can be explained by the presence of Crozet and Kerguelen Islands, whose shelves favour primary production by enriching the environment with iron, a limiting element for primary production in the Southern Ocean (Doty and Oguri, 1956; Blain et al., 2007). As such, recurrent blooms are observed downstream of these islands (Sokolov and Rintoul, 2007). Strass et al. (2002) also suggest that the higher chlorophyll-a concentrations observed in the PFZ are caused by a latitudinal band of strong mesoscale eddies following the PF. A shift in surface waters was observed between hydrologic region 5 (Figure 4 in green) and hydrologic region 6 (Figure 4 in light blue), the former having surface waters close to SASW and the latter having surface waters closer to AASW. Moreover, the PFZ was described as having the SAF as its northern border, which was already identified as hydrologic region 5's southern border, and the Polar Front (PF) as its southern border. The PF is known to rise north at the east of Kerguelen Plateau, which is seen in the southern border of hydrologic region 6, allowing us to identify it as the PF (Orsi et al., 1995). Even though sea surface salinity matches Racapé et al. (2010)'s description of the PFZ, with sea surface salinity below 33.85 (Figure 6b in light blue), we observe higher sea surface temperature maximum than expected, reaching almost 12°C instead of 9°C (Figure 6a in light blue). Finally, hydrologic region 7 (Figure 4a in blue) corresponds to the Antarctic Zone (AZ), having the PF as its northern border (Orsi et al., 1995). Sea surface temperature (Figure 6a in blue) doesn't exceed 4°C in this hydrologic region and sea surface salinity (Figure 6b in blue) is higher than 33.8, matching AZ's description made by Racapé et al. (2010). We observe similar mean chlorophyll-a concentrations in this region than in the SAZ and PFZ (Figure 6f in blue), even with the AZ being an HNLC zone and despite the highest maximum concentration observed in the PFZ. This can be explained by the fact that the hydrologic regions were defined only on open ocean zones where bathymetry reached 1000m and as such exclude neritic areas and island shelves, where chlorophyll-a concentration are up to a hundred times higher (Doty and Oguri, 1956).

Southern Indian Ocean hydrologic regions

The hydrologic regions obtained in the Southern Indian Ocean combine the epipelagic bioregions obtained by Longhurst (2010) and the mesopelagic biogeochemical provinces obtained by Reygondeau et al. (2018). Nevertheless, the different regions seem to correspond to a subdivision of the subtropical zone (STZ) defined by Orsi et al. (1995), with the STF as its southern boundary. The subdivision of the Subtropical Zone (STZ) seems to reflect the opposition between the influence of the subtropical Indian gyre and the seasonal Indian upwelling region identified by Reygondeau et al. (2018). Longhurst (2010) identified a single epipelagic biogeochemical province in the Southern Indian Ocean called the Indian South Subtropical Gyre Province (ISSG). By using the mesopelagic environment, Reygondeau et al. (2018) identified a subdivision in the subtropical Indian ocean, with the western hydrologic region 3 (Figure 4a in light orange) being a distinct mesopelagic biogeochemical province called a Subtropical Province (STRP), whereas the eastern hydrologic region 2 (Figure 4a in orange) is identified as one of the Subtropical Gyre Province. This subdivision can be explained by the lower mean sea surface salinity observed in hydrologic region 3 (Figure 6b in light orange) compared to hydrologic region 2 (Figure 6b in orange), from 35.5 to 35.7 respectively, and with maximum sea surface salinity reaching 36.14 in the eastern region (Figure 6b in orange) compared to 35.83 in the western region (Figure 6b in light orange). This lower salinity in the west can be explained by the influence of the southern branch of the South Equatorial Current, which forms the East Madagascar Current (Lutjeharms et al., 1981). The latter carries lower salinity surface water due to freshwater input from rainfall and rivers near Madagascar (Longhurst, 2010). Only hydrologic region 1 (Figure 4a in red) differs from the rest of the subtropical hydrologic regions by having a lower surface salinity than the STSW observed in hydrologic regions 2 and 3 (Figure 6b), with a mean surface salinity of 35.36 compared to a mean surface salinity of 35.69 for hydrologic region 2 and 35.5 for hydrologic region 3. However, the most striking difference is the rapid increase in salinity with depth in hydrologic region 1, reaching a maximum of 35.63 at 200 m depth, compared to hydrologic regions 2 and 3, which show a continuous decrease in salinity with depth. This subsurface salinity maximum identified by the fPCA (Figure 3c in blue) is explained by the formation of subtropical subsurface waters (SSW) within the Indian subtropical gyre between 200 and 500 m depth (Swallow et al., 1988), where evaporation exceeds precipitation (Schott and McCreary, 2001). These SSWs join the South Equatorial Current (SEC), which flows westwards between 6°S and 25°S to the east coast of Madagascar, where it splits into a northern and southern branch (Lutjeharms et al., 1981; Swallow et al., 1988). This westward circulation also explains the higher surface kinetic energy observed in this region (Figure 6d in red), as a sign of the SEC flowing above 30°S east of Madagascar. Finally, the spatial distribution of hydrologic region 4 (Figure 4a in yellow) corresponds to the distribution of the Subtropical Convergence Zone (STCZ). This zone is characterised by a strong decrease in salinity relative to subtropical waters around 35–40°S over a band of about 4–5° (Longhurst, 2010), its boundaries corresponding to the Northern Subtropical Front (NSTF) and the Southern Subtropical Front (SSFT, Belkin and Gordon, 1996). We observe this decrease in salinity within this hydrologic region, with the average salinity decreasing from 35.5 in hydrologic region 3 (Figure 6b in light orange) to an average salinity of 35 in hydrologic region 4 (Figure 6b in yellow). We can also observe a narrowing of the subtropical fronts north of Crozet, from a width of 5–8° latitude in the east to a width of barely 1° latitude in the west of the study area (Figure 4b). This narrowing corresponds to the 'Crozet Triple Front' observed by Belkin and Gordon (1996), where the topography constrains the hydrologic fronts crossing the area to a thin latitudinal band. Moreover, the high instability reflected by the high standard deviation observed could also result from the turbulences of the ARC. The widening observed in the eastern part of the study area can be explained by the northward curvature of the NSTF (Belkin and Gordon, 1996), opposite to its merging with the SSTF and SAF over Crozet Islands.

Conclusion

Regionalisation based on the functional decomposition of the PCA is a powerful method to identify hydrologic regions (Table II) in the Southern Ocean due to the well-segregated thermohaline structure along a latitudinal gradient resulting from ACC activity (Pauthenet et al., 2017). This allows the precise location of the various ACC-related fronts, as evidenced by the low standard deviation values and their concentration in thin latitudinal bands and could provide a powerful and accurate tool for identifying the geographic location of these hydrologic fronts without relying on the criteria defined in previous work (Sokolov and Rintoul, 2009). It also appears to be more accurate in its subdivision of the Southern Indian Ocean and the subtropical environment via differences in salinity and temperature at depth, probably related to the use of the full hydrographic structure of the water column instead of focusing either on the epipelagic or mesopelagic layer. Without the influence of great topographic structures, such as island shelves, over the flow of current, the transitions between the different Southern Indian Ocean regions are larger and less stable than those in the Southern Ocean, showing variability in time. The large band of high standard deviation seen in the western side around 40°S seems to correspond to the Agulhas Return Current, which could be useful to predict its spatial position in the future. It is likely that a method based on only one layer of the water column would not have allowed us to obtain such a subdivision of the Southern Indian Ocean, whereas the use of the functional analysis on the epipelagic and mesopelagic layers combined allowed us to synthesise the results obtained on both layers in other studies (Longhurst, 2010; Reygondeau et al., 2018). It would be interesting to be able to predict the evolution of these provinces in the context of a significantly warmer Southern Ocean (Purkey and Johnson, 2010; Comiso et al., 2017), to determine the spatial and temporal stability of the different zones identified by hydrologic regionalisation.

Table 2: Hydrologic regions and their characteristics defined in this study.

Region number	Region's name	Code	Fronts/currents associated
1	Tropical Zone	TZ	South Equatorial Current
2	Eastern Subtropical zone	ESTZ	Indian Subtropical Gyre
3	Western Subtropical zone	WSTZ	East Madagascar Current
4	Subtropical Convergence Zone	STCZ	NSTF-SSTF
5	Subantarctic Zone	SAZ	STF-SAF
6	Polar Frontal Zone	PFZ	SAF-APF
7	Antarctic Zone	AZ	APF

Acknowledgements

This work is part of the REPCCOAI programme (Réponses de l'écosystème pélagique aux changements climatiques de l'océan Austral et de l'Indien Sud) funded by the French National Oceanographic Fleet, IFREMER and IPEV. It is part of the Zone Atelier Antarctique of CNRS. This article is a contribution to the Pelagic Ecoregionalisation of the Indian Subantarctic Zone and was funded by Antarctic and Southern Ocean Coalition (ASOC). We would like to thank ASOC for funding the Master's degree internship that served as the basis of this article. We would also like to thank the OFB (Office français de la biodiversité) for their financial support as part of the project 'International coordination of the ecoregionalisation of the Subantarctic Indian pelagic zone for the extension of high-sea marine protected areas (MPAs) within the CCAMLR zone' (OFB-23-0266). This report is a contribution to the pelagic ecoregionalisation of the subantarctic (Makhado et al., 2019, 2023).

References

Anilkumar, N., A.J. Luis, Y.K. Somayajulu, V. Ramesh Babu, M.K. Dash, S.M. Pednekar, K.N. Babu, M. Sudhakar and P.C. Pandey. 2006. Fronts, water masses and heat content variability in the Western Indian sector of the Southern Ocean during austral summer 2004. *J. Mar. Syst.,* 63(1): 20–34. https://doi.org/10.1016/j.jmarsys.2006.04.009.

Ariza, A., A. Lebourges-Dhaussy, D. Nerini, E. Pauthenet, G. Roudaut, R. Assunção, E. Tosetto and A. Bertrand. 2023. Acoustic seascape partitioning through functional data analysis. *J. Biogeogr.*, 50(9): 1546–1560. https://doi.org/10.1111/jbi.14534.

Ariza, A., M. Lengaigne, C. Menkes, A. Lebourges-Dhaussy, A. Receveur, T. Gorgues, J. Habasque, M. Gutiérrez, O. Maury and A. Bertrand. 2022. Global decline of pelagic fauna in a warmer ocean. *Nat. Clim. Chang.*, 12: 928–934. https://doi.org/10.1038/s41558-022-01479-2.

Belkin, I.M. and A.L. Gordon. 1996. Southern Ocean fronts from the Greenwich meridian to Tasmania. *J. Geophys. Res. Oceans*, 101(C2): 3675–3696. https://doi.org/10.1029/95JC02750

Blain, S., B. Quéguiner, L. Armand, S. Belviso, B. Bombled, L. Bopp, A. Bowie, C. Brunet, C. Brussaard, F. Carlotti, U. Christaki, A. Corbière, I. Durand, F. Ebersbach, J.-L. Fuda, N. Garcia, L. Gerringa, B. Griffiths, C. Guigue, C. Guillerm, S. Jacquet, C. Jeandel, P. Laan, D. Lefèvre, C. Lo Monaco, A. Malits, J. Mosseri, I. Obernosterer, Y.-H. Park, M. Picheral, P. Pondaven, T. Remenyi, V. Sandroni, G. Sarthou, N. Savoye, L. Scouarnec, M. Souhaut, D. Thuiller, K. Timmermans, T. Trull, J. Uitz, P. van Beek, M. Veldhuis, D. Vincent, E. Viollier, L. Vong and T. Wagener. 2007. Effect of natural iron fertilization on carbon sequestration in the Southern Ocean. *Nature*, 446: 1070–1074. https://doi.org/10.1038/nature05700.

Charriaud, E. and L. Gamberoni. 1987. Hydrologic observations and geostrophic flows between Kerguelen and Amsterdam. Results of the KERAMS 1 campaign (16-20 February 1987). *Rapport Interne du Laboratoire d'Océanographie Physique du Muséum National d'Histoire Naturelle de Paris*.

Comiso, J.C., R.A. Gersten, L.V. Stock, J. Turner, G.J. Perez and K. Cho. 2017. Positive Trend in the Antarctic Sea Ice Cover and Associated Changes in Surface Temperature. *JCLI*, 30(6): 2251–2267. https://doi.org/10.1175/JCLI-D-16-0408.1.

Deacon, G.E.R. 1982. Physical and biological zonation in the Southern Ocean. *Deep Sea Res. I: Oceanographic Research Papers*, 29(1), 1–15. https://doi.org/10.1016/0198-0149(82)90058-9.

Doty, M.S. and M. Oguri. 1956. The Island Mass Effect. *ICES J. Mar. Sci.*, 22(1), 33–37. https://doi.org/10.1093/icesjms/22.1.33.

Godet, C., M. Robuchon, B. Leroy, C. Cotté, A. Baudena, O. Da Silva, S. Fabri-Ruiz, C. Lo Monaco, S. Sergi and P. Koubbi. 2020. Matching zooplankton abundance and environment in the Southern Indian Ocean and Southern Ocean. *Deep Sea Res. I: Oceanographic Research Papers*, 163: 103347. https://doi.org/10.1016/j.dsr.2020.103347.

Kolbe, M., F. Roquet, E. Pauthenet and D. Nerini. 2021. Impact of Thermohaline Variability on Sea Level Changes in the Southern Ocean. *J. Geophys. Res. Oceans*, 126(9), e2021JC017381. https://doi.org/10.1029/2021JC017381.

Longhurst, A.R. 2010. *Ecological Geography of the Sea*. Academic Press, London: 560pp.

Lutjeharms, J.R.E., N.D. Bang and C.P. Duncan. 1981. Characteristics of the currents east and south of Madagascar. *Deep Sea Res. I: Oceanographic Research Papers*, 28(9), 879–899. https://doi.org/10.1016/0198-0149(81)90008-X.

Lutjeharms, J.R.E. and C.E. da Silva. 2019. The Agulhas Return Current. In: Cochran, J.K., H.J. Bokuniewicz and P.L. Yager. (Eds.). *Encyclopedia of Ocean Sciences (Third Edition)*, 3: 236–247. https://doi.org/10.1016/B978-0-12-409548-9.11362-4.

Makhado, A.B., A. Lowther, P. Koubbi, I. Ansorge, C. Brooks, C. Cotté, R. Crawford, S. Dlulisa, F. d'Ovidio, S. Fawcet, D. Freeman, S. Grant, J. Huggett, M. Hindell, P.A. Hulley, S. Kirkman, T. Lamont, M. Lombard, M.J. Masothla, M.-A. Lea, W.C. Oosthuizen, F. Orgeret, R. Reisinger, T. Samaai, S. Sergi, K. Swadling, S. Somhlaba, A. Van de Putte, C. Von de Meden and D. Yemane. 2019. Expert Workshop on Pelagic Spatial Planning for the eastern subantarctic region (Domains 4, 5 and 6). Document *SC-CAMLR-38/BG/29*. CCAMLR, Hobart, Australia: 71 pp.

Makhado, A., P. Koubbi, J.A. Huggett, C. Cotté, R. Reisinger, K.M. Swadling, C. Azarian, C. Barnerias, F. d'Ovidio, L. Gauthier, E. Goberville, B. Leroy, A.T. Lombard, L. Muller, A. Van de Putte and workshop participants. 2023. Ecoregionalisation of the pelagic zone in the Subantarctic and Subtropical Indian Ocean. Document *SC-CAMLR-42/08*. CCAMLR, Hobart, Australia, 32 pp.

Orsi, A.H., T. Whitworth and W.D. Nowlin. 1995. On the meridional extent and fronts of the Antarctic Circumpolar Current. *Deep Sea Res. I: Oceanographic Research Papers,* 42(5): 641–673. https://doi.org/10.1016/0967-0637(95)00021-W.

Park, Y.-H., L. Gamberoni and E. Charriaud. 1993. Frontal structure, water masses, and circulation in the Crozet Basin. *J. Geophys. Res. Oceans*, 98(C7): 12361–12385. https://doi.org/10.1029/93JC00938.

Park, Y.-H., L. Gambéroni and E. Charriaud. 1991. Frontal structure and transport of the Antarctic Circumpolar Current in the South Indian Ocean sector, 40–80°E. *Mar. Chem.*, 35(1-4): 45–62. https://doi.org/10.1016/S0304-4203(09)90007-X.

Pauthenet, E. and D. Nerini. 2023. fda.oce: Functional Data Analysis of oceanographic profiles. R package version 0.1.0. https://github.com/EPauthenet/fda.oce.

Pauthenet, E., F. Roquet, G. Madec and D. Nerini. 2017. A Linear Decomposition of the Southern Ocean Thermohaline Structure. *J. Phys. Oceanogr.*, 47(1), 29–47. https://doi.org/10.1175/JPO-D-16-0083.1.

Pondaven, P., C. Fravalo, D. Ruiz-Pino, P. Tréguer, B. Quéguiner and C. Jeandel. 1998. Modelling the silica pump in the Permanently Open Ocean Zone of the Southern Ocean. *J. Mar. Syst.*, 17(1–4), 587–619. https://doi.org/10.1016/S0924-7963(98)00066-9.

R Core Team. 2022. R: A language and environment for statistical computing. R Foundation for Statistical Computing, Vienna, Austria. https://www.R-project.org/.

Racapé, V., C.L. Monaco, N. Metzl and C. Pierre. 2010. Summer and winter distribution of δ13CDIC in surface waters of the Southern Indian Ocean [20°S-60°S]. *Tellus B: Chem. Phys. Meteorol.*, 62(5): 660–673. https://doi.org/10.1111/j.1600-0889.2010.00504.x.

Ramsay, J.O. and B.W. Silverman. 2015. Functional Data Analysis. In: Wright, J.D. (Ed.). *International Encyclopedia of the Social & Behavioral Sciences (Second Edition)*. Elsevier, Oxford, pp. 514–518. https://doi.org/10.1016/B978-0-08-097086-8.42046-5.

Reygondeau, G., L. Guidi, G. Beaugrand, S.A. Henson, P. Koubbi, B.R. MacKenzie, T.T. Sutton, M. Fioroni and O. Maury. 2018. Global biogeochemical provinces of the mesopelagic zone. *J. Biogeogr.*, 45(2): 500–514. https://doi.org/10.1111/jbi.13149.

Schott, F.A. and J.P. McCreary. 2001. The monsoon circulation of the Indian Ocean. Progr. Oceanogr., 51(1): 1–123. https://doi.org/10.1016/S0079-6611(01)00083-0.

Sokolov, S. and S.R. Rintoul. 2007. On the relationship between fronts of the Antarctic Circumpolar Current and surface chlorophyll concentrations in the Southern Ocean. *J. Geophys. Res. Oceans*, 112(C7). https://doi.org/10.1029/2006JC004072.

Strass, V.H., A.C. Naveira Garabato, R.T. Pollard, H.I. Fischer, I. Hense, J.T. Allen, J.F. Read, H. Leach and V. Smetacek. 2002. Mesoscale frontal dynamics: shaping the environment of primary production in the Antarctic Circumpolar Current. *Deep Sea Res. II: Top. Stud. Oceanogr.*, 49(18): 3735–3769. https://doi.org/10.1016/S0967-0645(02)00109-1.

Swallow, J., M. Fieux and F. Schott. 1988. The boundary currents east and north of Madagascar: 1. Geostrophic currents and transports. *J. Geophy. Res. Oceans*, 93(C5): 4951–4962. https://doi.org/10.1029/JC093iC05p04951.

Tibshirani, R., G. Walther and T. Hastie. 2001. Estimating the Number of Clusters in a Data Set via the Gap Statistic. *J. R. Stat. Soc. Ser. B: Stat. Methodol.*, 63(2): 411–423.

Wickham, H. 2016. ggplot2: Elegant Graphics for Data Analysis. Springer-Verlag New York.

Appendix A

Table A1: Table of selected environmental variables and associated information.

Environmental variable	Source and products	Spatial resolution (°)	Time resolution
Temperature (°C)	In situ observation data. High resolution data: Copernicus Marine Environmental Monitoring. Service website (http://marine.copernicus.eu/): "GLOBAL_REANALYSIS_PHY_001_031"	0.25	Monthly
Salinity (psu)	In situ observation data. Area-wide data: Copernicus Marine Environmental Monitoring Service website (http://marine.copernicus.eu/): "GLOBAL_REANALYSIS_PHY_001_031"	0.25	Monthly
Kinetic energy	Copernicus Marine Environmental Monitoring Service website (http://marine.copernicus.eu/): "GLOBAL_REANALYSIS_PHY_001_031", calculated via the values of zonal and meridional velocity.	0.25	Monthly
Mix-layer depth (m)	Copernicus Marine Environmental Monitoring Service website (http://marine.copernicus.eu/): "GLOBAL_REANALYSIS_PHY_001_031"	0.25	Monthly
Chlorophyll-a concentration (mg.m-3)	Copernicus Marine Environmental Monitoring Service website (http://marine.copernicus.eu/): "GLOBAL_MULTIYEAR_BGC_001_029"	0.25	Monthly
Oxygen concentration (mmol.m-3)	Copernicus Marine Environmental Monitoring Service website (http://marine.copernicus.eu/): "GLOBAL_MULTIYEAR_BGC_001_029"	0.25	Monthly